Journal of Organometallic Chemistry 694 (2009) 1161–1171

Contents lists available at ScienceDirect

Journal of Organometallic Chemistry

journal homepage: www.elsevier.com/locate/jorganchem

Synthesis, structure, electrochemistry, and Mössbauer effect studies of (ring)Fe complexes (ring = Cp, Cp*, and C_6H_7). Photochemical replacement of benzene in the cyclohexadienyl complex $[(\eta^5\text{-}C_6H_7)Fe(\eta\text{-}C_6H_6)]^+$

Piero Zanello [a,*], Rolfe H. Herber [b,*], Alexander R. Kudinov [c,*], Maddalena Corsini [a], Fabrizia Fabrizi de Biani [a], Israel Nowik [b], Dmitry A. Loginov [c], Mikhail M. Vinogradov [c], Lidia S. Shul'pina [c], Igor A. Ivanov [c], Anna V. Vologzhanina [c]

[a] Dipartimento di Chimica, University of Siena, Via A. De Gasperi 2, 53100 Siena, Italy
[b] Racah Institute of Physics, The Hebrew University, 91904 Jerusalem, Israel
[c] A.N. Nesmeyanov Institute of Organoelement Compounds, 28 ul. Vavilova, 119991 Moscow, GSP-1, Russian Federation

ARTICLE INFO

Article history:
Received 30 July 2008
Received in revised form 12 September 2008
Accepted 22 September 2008
Available online 27 September 2008

Dedicated to Professor Christoph Elschenbroich in recognition of his fundamental contributions to organometallics

Keywords:
Crystal structures
Electrochemistry
Mössbauer spectroscopy
Sandwich iron compounds

ABSTRACT

Visible light irradiation of cation $[(\eta^5\text{-}C_6H_7)Fe(\eta\text{-}C_6H_6)]^+$ (**1**$^+$) in acetonitrile results in substitution of the benzene ligand giving the labile acetonitrile derivative $[(\eta^5\text{-}C_6H_7)Fe(MeCN)_3]^+$ (**2a**$^+$). The stable isonitrile and phosphite complexes $[(\eta^5\text{-}C_6H_7)FeL_3]^+$ [L = ^{t}BuNC (**2b**$^+$), $P(OMe)_3$ (**2c**$^+$), $P(OEt)_3$ (**2d**$^+$)] were obtained by reaction of **1** with L in MeCN. The structures of **2c**PF_6, $[CpFe(\eta\text{-}C_6H_6)]PF_6$ (**3**PF_6), and $Cp^*Fe(\eta\text{-}C_6H_6)]PF_6$ (**4**PF_6) were determined by X-ray diffraction.

The redox activity of the cyclohexadienyl complexes **1**$^+$, **2b**$^+$–**2d**$^+$ has been investigated by electrochemical techniques and compared with that of the related cyclopentadienyl complexes **3**$^+$ and **4**$^+$. DFT calculations of the redox potentials and the respective geometrical changes were performed.

Variable temperature Mössbauer (ME) spectroscopy has elucidated the relationship between structure and formal oxidation state of the iron atom in these complexes. In the case of **3**$^+$ an unexpected pair of crystallographic changes has been observed and interpreted in terms of both a second and first order phase transition. The mean-square-amplitude-of-vibration of the metal atom has been compared between the ME and X-ray data. ME measurements in a magnetic field have shown that in **4**$^+$ the quadrupole splitting is positive as it is in ferrocene.

1. Introduction

The cyclopentadienyl complex $[CpFe(\eta\text{-}C_6H_6)]^+$ (**3**$^+$) is known to replace the benzene ligand by 2- and 6-electron donors under visible light irradiation [1,2]. We have found earlier that the (tetramethylcyclobutadiene)cobalt cation $[(\eta\text{-}C_4Me_4)Co(\eta\text{-}C_6H_6)]^+$ reacts in a similar manner [3,4]. Due to these reactions the benzene complexes are useful synthons of the cationic fragments $[CpFe]^+$ and $[(\eta\text{-}C_4Me_4)Co]^+$, which was proven by their successful application for the synthesis of sandwich, triple-decker, and cluster complexes [5–8].

The (cyclohexadienyl)iron fragment $[(\eta^5\text{-}C_6H_7)Fe]^+$ is isolobal with $[CpFe]^+$ and $[(\eta\text{-}C_4Me_4)Co]^+$ suggesting photochemical lability of the benzene complex $[(\eta^5\text{-}C_6H_7)Fe(\eta\text{-}C_6H_6)]^+$ (**1**$^+$). Indeed, as we have recently shown, **1**$^+$ undergoes arene exchange under visible light irradiation with the formation of derivatives $[(\eta^5\text{-}C_6H_7)Fe(\eta\text{-}C_6R_6)]^+$ [9]. Subsequent hydride abstraction allows to obtain unsymmetrical bis(arene) complexes $[(\eta\text{-}C_6H_6)Fe(\eta\text{-}C_6R_6)]^{2+}$. Herein we report the reactions of **1**$^+$ with 2-electron ligands [10] as well as the results of structural, electrochemical and Mössbauer effect studies of (cyclohexadienyl)iron complexes and other related species.

2. Results and discussion

2.1. Reactions

We have found that visible light irradiation of the (cyclohexadienyl)(benzene) complex **1**$^+$ in acetonitrile results in benzene replacement giving the labile acetonitrile derivative $[(\eta^5\text{-}C_6H_7)Fe(\text{-}MeCN)_3]^+$ (**2a**$^+$) (Scheme 1). Complex **2a**$^+$ is moderately stable in acetonitrile solution at 0 °C but rapidly decomposes at room temperature.

The stable tris(ligand) complexes **2b**$^+$–**d**$^+$ were prepared by irradiation of **1**$^+$ with ^{t}BuNC and $P(OR)_3$ (R = Me, Et) in acetonitrile.

* Corresponding authors.
E-mail addresses: zanello@unisi.it (P. Zanello), herber@vms.huji.ac.il (R.H. Herber), arkudinov@ineos.ac.ru (A.R. Kudinov).

0022-328X/$ - see front matter © 2008 Elsevier B.V. All rights reserved.
doi:10.1016/j.jorganchem.2008.09.028

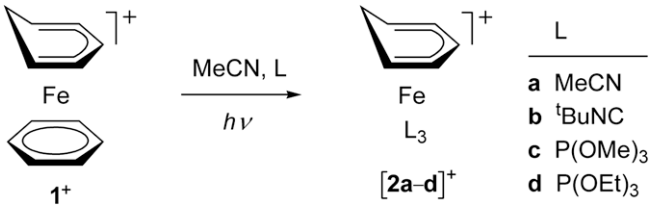

Scheme 1.

The isonitrile complex **2b**PF_6 is indefinitely stable in air. However, the phosphite derivatives **2c**PF_6 and **2d**PF_6 are air-stable only for a short period of time but decompose upon prolonged contact with air, possibly owing to oxidation. Noteworthy, similar reactions of the cyclopentadienyl analogue $[CpFe(\eta\text{-}C_6H_6)]^+$ (**3**$^+$) lead to complexes $[CpFe(MeCN)L_2]^+$ (L = RNC, $P(OR)_3$), containing only two phosphite or isocyanide ligands [11].

2.2. X-ray diffraction study

The structures of **2c**PF_6, $[CpFe(\eta\text{-}C_6H_6)]PF_6$ (**3**PF_6) and $[Cp^*Fe(\eta\text{-}C_6H_6)]PF_6$ (**4**PF_6) were determined by X-ray diffraction. Cation **2c**$^+$ has the expected half-sandwich structure, Fig. 1. The folding angle of the C_6H_7 ligand along the C2···C6 line is equal to 43.0°. This value is larger than that in the isonitrile analogue **2b**PF_6 (33.9°) [10]. Moreover, the Fe···C_6H_7 distance in **2c**$^+$ (1.647 Å) is longer than that in **2b**$^+$ (1.625 Å). The increase of the folding angle and the Fe···C_6H_7 distance for cation **2c**$^+$ is conceivably due to steric and electronic effects of phosphite ligands.

The structure of the cation **3**$^+$ was studied earlier, but these experiments were carried out for complexes including large molecules, such as cyclodextrin and bis(maleonitriledithiolato)-nickel [12,13]. We conducted X-ray studies of **3**PF_6 at 100 K, Fig. 2, and 296 K.

According to the present results, the monocation shows phase transformation with decrease of temperature. In both cases the substance belongs to monoclinic crystal system, although it has space group *C*2/*c* or *P*2$_1$, for the high- and low temperature forms, respectively. The phase change for **3**PF_6 obey the rule that the high temperature form is higher in symmetry than the low temperature one. The low temperature modification has four crystallographically independent anions and cations. There exists only one anion and two cations (in special positions) for the high temperature form, but both cations are highly disordered as can be seen from Fig. 3. The Fe···C_6H_6 distances are equal to 1.533–1.543 and 1.543–1.574 Å for the high and low temperature forms, the Fe···Cp distances are longer, 1.648–1.649 and 1.617–1.665 Å, and the dihedral angles between C_6H_6 and Cp planes are 2.8–3.6 and 0.7–1.8°, respectively. So, these cations have the same geometry as previously reported substances with Fe···C_6H_6 and Fe···Cp distances of 1.494–1.566 and 1.598–1.657 Å and C_6H_6/Cp angle of 1.5–2.4° [12,13].

As it can be seen from Table 1, crystal parameters *a*, *b*, and *c* (after some transformations) for **3**PF_6 differ only slightly, as can be expected from the temperature decrease. Taking into account that the low temperature phase was obtained from the high temperature ones just by cooling of the sample under N_2 without

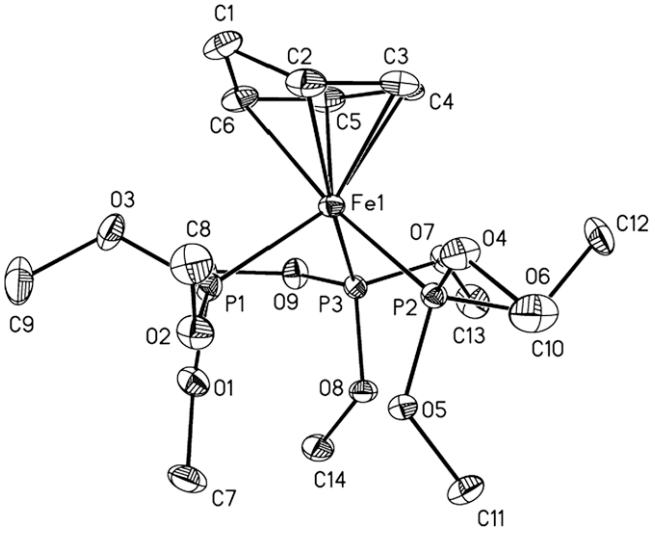

Fig. 1. Structure of cation **2c**$^+$ in **2c**PF_6. Ellipsoids are shown at 50% level. Selected bond lengths [Å] and angles [°]: Fe1–C2 2.195(3), Fe1–C3 2.104(3), Fe1–C4 2.115(3), Fe1–C5 2.114(3), Fe1–C6 2.202(3), Fe1–P1 2.1619(9), Fe1–P2 2.1647(8), Fe1–P3 2.1681(8), C1–C2 1.520(5), C2–C3 1.402(5), C3–C4 1.405(4), C4–C5 1.431(5), C5–C6 1.397(5), C1–C6 1.520(5), C2–C1–C6 102.5(3), C1–C2–C3 118.3(3), C2–C3–C4 120.7(3), C3–C4–C5 117.3(3), C4–C5–C6 119.8(3), C5–C6–C1 118.9(3).

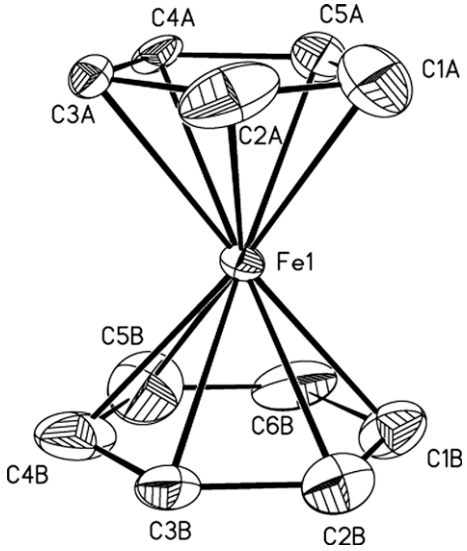

Fig. 2. Structure of cation **3**$^+$ in **3c**PF_6 (low temperature modification, only one independent molecule is shown). Ellipsoids are shown at 50% level. Selected bond lengths [Å]: Fe1–C1A 1.972(6), Fe1–C2A 2.013(5), Fe1–C3A 2.071(4), Fe1–C4A 2.067(4), Fe1–C5A 2.006(5), Fe1–C1B 2.072(4), Fe1–C2B 2.067(5), Fe1–C3B 2.076(5), Fe1–C4B 2.091(5), Fe1–C5B 2.096(5), Fe1–C6B 2.086(4).

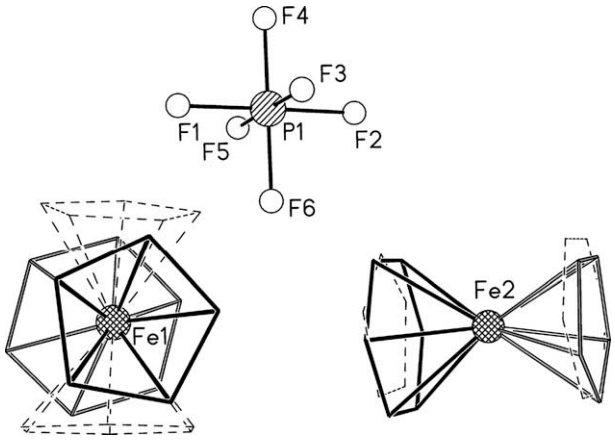

Fig. 3. Molecular view of **3**PF_6. The alternative positions of the cations are shown by dashed lines. The occupancies of both positions are equal to 0.5.

Table 1
Crystal data and structure refinement parameters for **2c**PF_6, **3**PF_6, and **4**PF_6

Compound	**2c**PF_6	**3**PF_6 low temperature	**3**PF_6 high temperature	**4**PF_6
Empirical formula	$C_{15}H_{34}F_6FeO_9P_4$	$C_{11}H_{11}F_6FeP$	$C_{11}H_{11}F_6FeP$	$C_{16}H_{21}F_6FeP$
Formula mass	652.15	344.02	344.02	414.15
Crystal colour, habit	Yellow prism	Yellow prism	Yellow prism	Yellow plate
Crystal size [mm]	0.26 × 0.19 × 0.13	0.47 × 0.23 × 0.21	0.65 × 0.34 × 0.21	0.43 × 0.20 × 0.08
Crystal system	Monoclinic	Monoclinic	Monoclinic	Orthorhombic
Space group	*Pc*	$P2_1$	*C*2/*c*	*Pnma*
a (Å)	11.3941(6)	9.4106(6)	28.170(2)	15.4960(9)
b (Å)	9.0581(5)	9.4629(6)	9.5641(7)	14.9752(8)
c (Å)	15.9874(9)	26.5996(17)	9.5710(7)	7.2445(4)
α (°)	90	90	90	90
β [°]	129.4200(10)	94.1150(10)	105.8760(10)	90
γ (°)	90	90	90	90
V (Å^3)	1274.68(12)	2362.6(3)	2480.2(3)	5503(4)
Z	2	8	8	4
D (calcd.) (g cm^{-3})	1.699	1.934	1.843	1.636
Diffractometer	Bruker SMART APEX2 CCD			
Temperature (K)	100	100	296	100
Radiation	Mo Kα (λ = 0.71073)			
$2\theta_{max}$ (°)	56.00	53.00	65.00	52.00
Absorption coefficient μ (Mo Kα) (cm^{-1})	9.30	14.70	14.01	10.48
Absorption correction	Multi-scan			
$T_{max.}$ and $T_{min.}$	0.889 and 0.806	0.738 and 0.680	0.7475 and 0.5729	0.924 and 0.780
Completeness (%)	99.9	99.4	98.0	97.8
Structure solution	Direct method			
Refinement method	Full-matrix least-squares on F^2			
Collected reflections	18694	20284	17210	10225
Independent reflections [$R_{(int)}$]	6118 (0.0231)	9725 (0.0319)	4417 (0.0230)	1676 (0.0711)
Observed reflections [$I > 2\sigma(I)$]	5988	8058	3387	1558
Parameters	325	601	91	138
R_1 (on *F* for observed reflections)	0.0342	0.0576	0.0796	0.0936
wR_2 (on F^2 for all reflections)	0.0816	0.1134	0.2161	0.2264
Weighting scheme	$w^{-1} = \sigma^2(F_o^2) + (aP)^2 + bP,\ P = 1/3(F_o^2 + 2F_c^2)$			
A	0.0200	0.0070	0.1000	0.0000
B	3.0000	15.5200	12.0000	15.5200
F(000)	672	1376	1376	848
Goodness-of-fit (GOF)	0.994	1.007	1.006	1.006
Largest difference peak and hole [e Å^{-3}]	0.901 and − 0.640	1.622 and − 0.886	1.250 and − 0.765	0.924 and − 1.772

decomposition of the monocrystal, one may suggest that this change belongs to the phase change of the second order. Fig. 4 represents a fragment of crystal packing for these phases. One may find the following discrepancies in the packing of anions and cations: as for cations, not only disordered molecules become ordered ones, but the angle between the Cp···Fe···C_6H_6 axes of neighboring molecules changes. The anion distribution also differs for the two phases. The F–P–F bonds of neighboring anions are parallel at room temperature, and are not (with the angles exceeding 38.6–54.7°) at low temperature, and at the same time they move so that P atoms are situated approximately on the line parallel with the *c* crystal axes. As a result of this movement surrounding of cations and anions in these phases is different. It is interesting to note that both modifications may be approximated by body-centered cubic distribution of anions and cations subcell with molecular coordination numbers (MCN) equal to 14. In the case of the low temperature form, all cations are surrounded by 8 cations and 6 anions, whilst anions contact with 8 anions and 6 cations. In the structure of the high temperature form only one cation (with the angle between disordered Cp···Fe···C_6H_6 bonds equal to 90°) has 8 neighboring cations and 6 anions and the second cation as well as the anion are surrounded by 8 anions and 6 cations. The data obtained suggest that **3**PF_6 undergoes a phase transition at temperatures below 0 °C, and this transformation belongs to a type of "order-disorder" change. Further evidence for this phenomenon will be considered in discussion of the Mössbauer effect data, below.

Finally, the molecular structure of cation **4**$^+$ (at 100 K) is illustrated in Fig. 5. The Fe···C_6H_6 distance (1.538 Å) is slightly shorter and the Fe···Cp distance (1.668 Å) is slightly longer than the corresponding distances in the parent cation **3**$^+$ at the same temperature. The shortening of the former is caused by stronger Fe → C_6H_6 back donation due to the donor effect of the methyl groups. The strengthening of the Fe–C_6H_6 bond is accompanied by loosening of the Fe–Cp bond. The dihedral angle between the C_6H_6 and Cp planes in **4**$^+$ (1.9°) is slightly bigger than that in **3**$^+$.

2.3. Electrochemistry

The electrochemical behaviour of complexes [$CpFe^{II}(\eta^6$-arene)]$^+$ is long known [14], as that of the three-legged piano-stool [$CpFe^{II}(L_3)$]$^+$ is [15]. In contrast, the redox activity of the isoelectronic analogues [$(\eta^5$-$C_6H_7)Fe^{II}(\eta^6$-arene)]$^+$ and [$(\eta^5$-$C_6H_7)Fe^{II}(L_3)$]$^+$ has been less investigated [16]. In this light we report here the electrochemical behaviour of complexes **1**$^+$, **2b**$^+$–**d**$^+$, **3**$^+$ and **4**$^+$.

As a starting point, Fig. 6 compares the cyclic voltammetric behaviour of the classical [$CpFe^{II}(\eta$-$C_6H_6)$]$^+$ (**3**$^+$) with that of the isoelectronic [$(\eta^5$-$C_6H_7)Fe^{II}(\eta$-$C_6H_6)$]$^+$ (**1**$^+$) in CH_2Cl_2 solution, at −20 °C.

Complexes [$(\eta$-$C_5R_5)Fe^{II}(\eta$-$C_6H_6)$]$^+$ undergo the Fe(II)/Fe(I) reduction displaying extents of chemical reversibility which are function of the solvent [14c]. Under the present experimental conditions, analysis of the cyclic voltammetric behaviour of **3**$^+$ with scan rates progressively increasing from 0.02 V s^{-1} to 2.0 V s^{-1} shows that the current ratio i_{pa}/i_{pc} is constantly minor than 1 (for instance the i_{pa}/i_{pc} ratio is 0.6 at 0.2 V s^{-1} and increases to 0.8 at 2 V s^{-1}), thus indicating that the reduction process is complicated

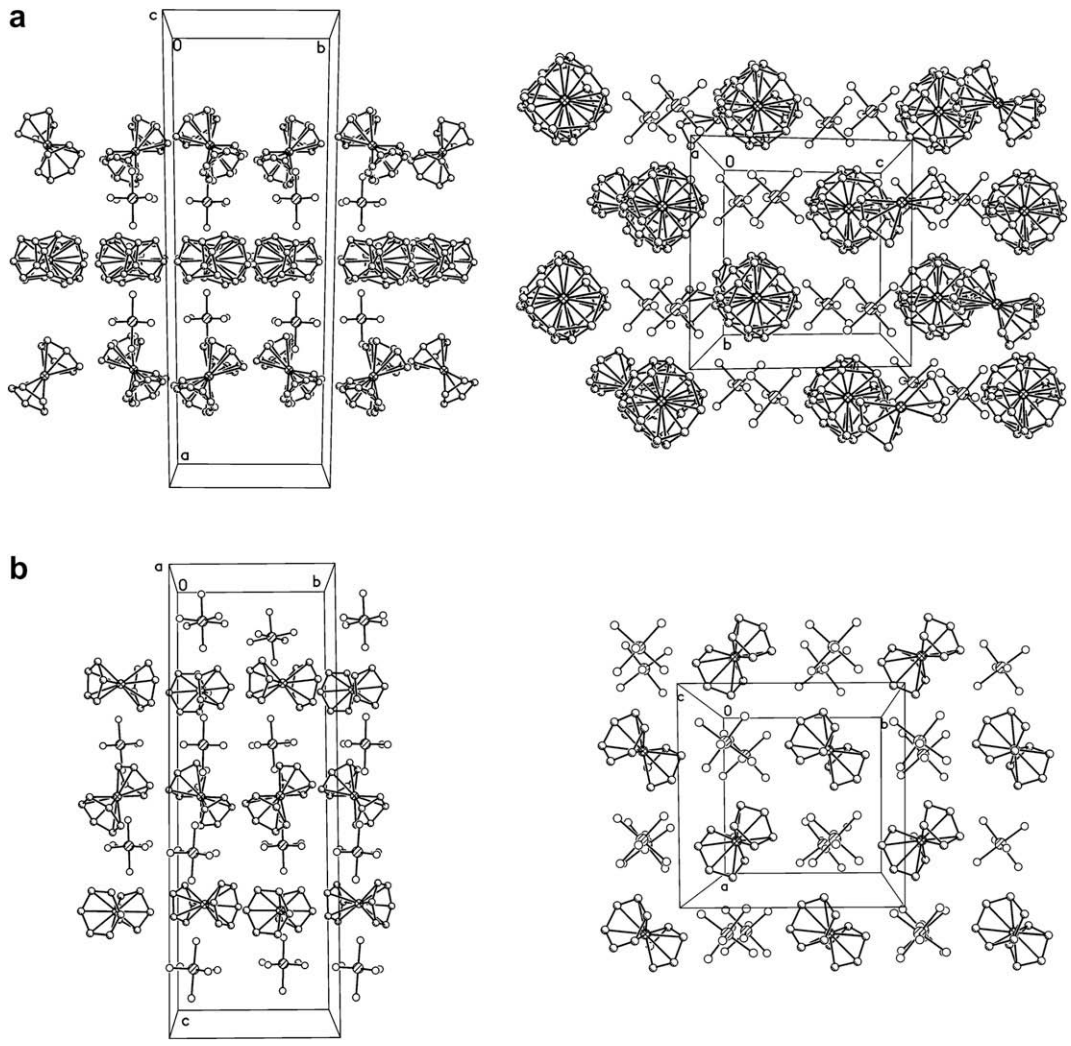

Fig. 4. Fragment of crystal packing in the structure of $\mathbf{3}PF_6$ at 296 K (a) and 100 K (b), respectively.

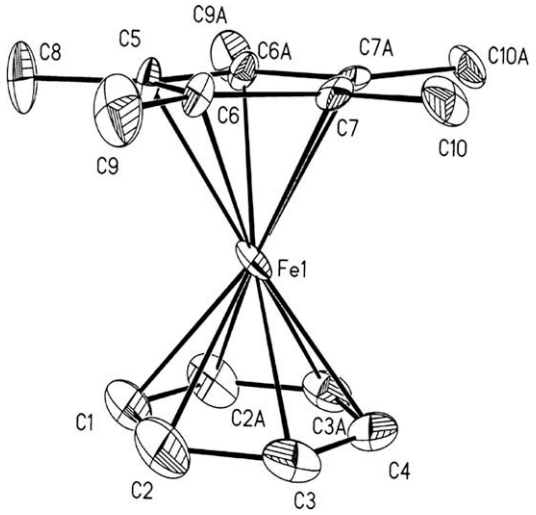

Fig. 5. Structure of cation $\mathbf{4}^+$ in $\mathbf{4}PF_6$. Ellipsoids are shown at 50% level. Selected bond lengths [Å]: Fe1–C1 2.099(13), Fe1–C2 2.094(9), Fe1–C3 2.084(9), Fe1–C4 2.095(13), Fe1–C5 2.050(12), Fe1–C6 2.062(8), Fe1–C7 2.073(8), C1–C2 1.425(12), C2–C3 1.411(14), C3–C4 1.413(12), C5–C6 1.427(10), C6–C7 1.435(11).

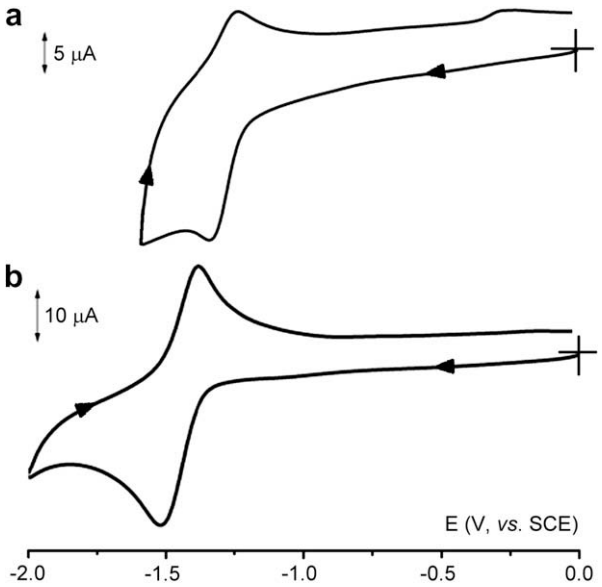

Fig. 6. Cyclic voltammograms recorded at a gold electrode in CH_2Cl_2 solution of: (a) $\mathbf{3}PF_6$ (1.5×10^{-3} mol dm^{-3}); (b) $\mathbf{1}PF_6$ (0.9×10^{-3} mol dm^{-3}). $[NBu_4][PF_6]$ (0.2 mol dm^{-3}) supporting electrolyte. Scan rate 0.2 V s^{-1}. T = −20 °C.

by following chemical reactions. Assuming the occurrence of a first order chemical complication, a lifetime of about 4 s can be assigned to the neutral Fe(I) species $[CpFe(\eta\text{-}C_6H_6)]^0$ [17]. As easily deducible, even faster chemical complications also accompany the one-electron reduction of $\mathbf{1}^+$. As a matter of fact, under the above assumptions, the electrogenerable $[(\eta^5\text{-}C_6H_7)Fe^{I}(\eta\text{-}C_6H_6)]^0$ results notably shorter-lived, its lifetime resulting of about 0.7 s.

As reported in Table 2, the reduction process of the cyclohexadienyl species $\mathbf{1}^+$ proceeds at a formal electrode potential less negative by about 0.1 V with respect to the isoelectronic cyclopentadienyl species.

$\mathbf{1}^+$ also exhibits an irreversible oxidation, which, as illustrated in Fig. 7, particularly at low temperature, is accompanied by strong adsorption effects.

In this connection, aromatic organo-iron compounds have a rich reactivity coupled with redox activity. For example they can undergo deligation upon reduction, nucleophilic addition or elimination reaction upon oxidation [14b,g]. For these reasons it is not straightforward to make a guess on the nature of the electrodeposited species following the actual oxidation process. By way of speculation, it cannot be ruled out that, upon oxidation, $[(\eta^5\text{-}C_6H_7)Fe^{II}(\eta\text{-}C_6H_6)]^+$ might convert to the bis(arene) complex $[(\eta\text{-}C_6H_6)_2Fe]^+$, through a deprotonation step. In fact, it is known that the arene-methylated dications $[(\eta\text{-}C_6R_6)_2Fe]^{2+}$ can be chemically reduced to the corresponding cyclohexadienyl monocations $[(\eta^5\text{-}C_6R_6H)Fe(\eta\text{-}C_6R_6)]^+$ through the intermediate formation of $[(\eta\text{-}C_6R_6)_2Fe]^+$ [18]. Under this hypothesis, the single-asterisked peak-system in Fig. 7 arising from the original oxidation could be due to the electron-transfer process $[(\eta\text{-}C_6H_6)_2Fe]^{2+/+}$ of the electrodeposed bis-arene species, as well as the doubly-asterisked process could be due to the subsequent $[(\eta\text{-}C_6H_6)_2Fe]^{+/0}$ step. Since the actual $E^{\circ\prime} = +0.84$ V recorded in CH_2Cl_2 solution at −25 °C for the couple $[(\eta\text{-}C_6H_6)_2Fe]^{2+/+}$ significantly departs from the $E^{\circ\prime}$ value of +0.16 V (versus SCE), which one could extrapolate from the $E^{\circ\prime}$ values for the reductions of $[(\eta\text{-}C_6H_3Me_3)_2Fe]^{2+}$ and $[(\eta\text{-}C_6Me_6)_2Fe]^{2+}$ in MeCN solution at +25 °C (assuming that the inductive effects of the methyl groups are additive) [19], we must assume that the markedly different experimental conditions might account for such a discrepancy. The same would hold for the actual value of E_p = −0.73 V for the couple $[(\eta\text{-}C_6H_6)_2Fe]^{+/0}$ with respect to the value of −1.07 V for the same couple under the mentioned different experimental conditions [19].

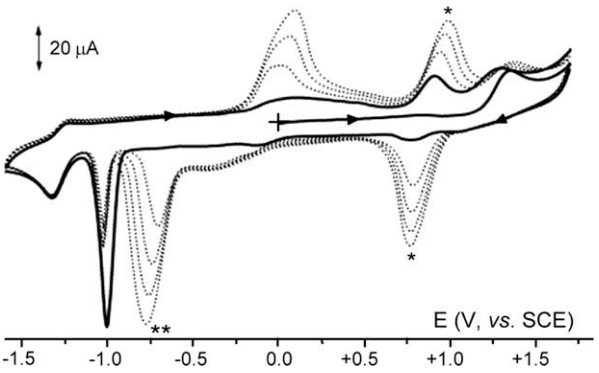

Fig. 7. Multiscan cyclic voltammetric profile recorded at a gold electrode in CH_2Cl_2 solution of $\mathbf{1}PF_6$ (0.9×10^{-3} mol dm^{-3}). $[NBu_4][PF_6]$ (0.2 mol dm^{-3}) supporting electrolyte. Scan rate 0.2 V s^{-1}. T = −20 °C. (–) First cycle.

Since the electrodeposition is obtained only on gold electrodes (and at low temperature), this might suggest that a chemisorption is active rather than a simple absorption, so that a significant shift of the potential values is not unexpected. Finally, it is noted that the electrochemical deposition of organo-iron compounds can be regarded as a very cheap and easy alternative of MOCVD for the handling of highly dispersed iron supported catalysts, which are widely used in industrial applications [20].

Table 2
Formal electrode potentials (V, vs. SCE), peak-current ratios, and peak-to-peak separations (mV) for the redox processes exhibited by the complexes under study in different solvents and at different temperatures (°C)

Complex	Reduction processes			Oxidation processes			Solvent	Temperature	Reference
	$E^{\circ\prime}_{(+/0)}$	i_{pa}/i_{pc}	ΔE_p	$E^{\circ\prime}_{(+/2+)}$	i_{pc}/i_{pa}	ΔE_p			
$[CpFe(\eta\text{-}C_6H_6)]^+$ ($\mathbf{3}^+$)	−1.44	0.8[a]	115[a]	–	–	–	CH_2Cl_2	−20	[b]
	−1.36	0.8[c]	–	–	–	–	DMF	−30	13 [d], [f]
	−1.39	0.7[a]	98[a]	–	–	–	CH_2Cl_2	+20	[b]
	−1.30	1	–	–	–	–	Me_2CO	–	13 [c]
	−1.36	0.4	–	–	–	–	MeCN	–	13 [c]
$[Cp^*Fe(\eta\text{-}C_6H_6)]^+$ ($\mathbf{4}^+$)	−1.73	0.5[a]	100	+1.70[d]	–	–	CH_2Cl_2	−20	[b]
	−1.64	0.9[c]	–	–	–	–	DMF	−30	13 [d], [f]
	−1.68	0.4[a]	75	+1.72[d]	–	–	CH_2Cl_2	+20	[b]
	−1.58	1	–	–	–	–	Me_2CO	–	13 [c]
	−1.67	1	–	–	–	–	MeCN	–	13 [c]
$[(\eta^5\text{-}C_6H_7)Fe(\eta\text{-}C_6H_6)]^+$ ($\mathbf{1}^+$)	−1.35	0.4[a]	85	+1.35[d]	–	–	CH_2Cl_2	−20	[b]
	−1.33	0.3[e]	160[e]	–	–	–	CH_2Cl_2	+20	[b]
$[(\eta^5\text{-}C_6H_7)Fe(^tBuNC)_3]^+$ ($\mathbf{2b}^+$)	–	–	–	+1.07	0.4[g]	270[g]	CH_2Cl_2	−20	[b]
	–	–	–	+1.12[d]	–	–	CH_2Cl_2	+20	[b]
$[(\eta^5\text{-}C_6H_7)Fe\{P(OMe)_3\}_3]^+$ ($\mathbf{2c}^+$)	–	–	–	+1.04	0.2[a]	134[a]	CH_2Cl_2	−20	[b]
	–	–	–	+1.05	0.4[e]	124[e]	CH_2Cl_2	+20	[b]
$[(\eta^5\text{-}C_6H_7)Fe\{P(OEt)_3\}_3]^+$ ($\mathbf{2d}^+$)	–	–	–	+1.05[d]	–	–	CH_2Cl_2	−20	[b]
	–	–	–	+1.03[d]	–	–	CH_2Cl_2	+20	[b]
$[CpFe^{II}\{(POMe)_3\}_3]^+$	−1.73[d]	–	–	–	–	–	DMF	−35	14 [b]
$[CpFe^{II}\{(POPh)_3\}_3]^+$	−1.2	0.6[h]	–	–	–	–	DMF	−35	14 [b]
$[CpFe^{II}\{(PMe)_3\}_3]^+$	–	–	–	+0.71	–	170	CH_2Cl_2	+25	14 [a]
	−2.05	0.1[h]	–	–	–	–	DMF	−35	14 [a]

[a] Measured at 0.2 V s^{-1}.
[b] Present work.
[c] Measured at 0.3 V s^{-1}.
[d] Peak-potential for irreversible processes.
[e] Measured at 2.0 V s^{-1}.
[f] Difficult to be determined accurately because of the closeness of the solvent discharge.
[g] Measured at 20.4 V s^{-1}.
[h] Measured at 1.0 V s^{-1}.

Let us now pass to the cyclohexadienyl piano-stool complexes **2b**$^+$**–d**$^+$. In this connection it must be considered that a few related cyclopentadienyl piano-stool species, such as $[CpFe^{II}(PMe_3)_3]^+$ and $[Cp^*Fe^{II}(dppe)X]^+$, afford a reversible $Fe^{II/III}$ oxidation [15a,c], whereas the $Fe^{II/I}$ reduction in $[CpFe^{II}(PR_3)_3]^+$ complexes is affected by chemical complications [15b]. The present cyclohexadienyl complexes $[(\eta^5\text{-}C_6H_7)Fe^{II}(L)_3]^+$ undergo an oxidation process which is coupled to chemical complications, the rate of which however is highly dependent upon the nature of the basal ligand L. As a matter of fact, while **2d**$^+$ exhibits a quite irreversible oxidation process, **2c**$^+$ and **2b**$^+$ give rise to partially chemically reversible anodic processes, having however different stabilities in their Fe(III) oxidation states, or: $[(\eta^5\text{-}C_6H_7)Fe\{P(OMe)_3\}_3]^{2+}$, $t_{1/2} \approx 0.2$ s; $[(\eta^5\text{-}C_6H_7)Fe(^t\text{BuNC})_3]^{2+}$, $t_{1/2} \approx 0.05$ s (see Fig. S1 in Supplementary material).

In conclusion, the cyclohexadienyl piano-stool Fe(III) complexes are markedly less stable than the isoelectronic cyclopentadienyl analogues, as on the other hand happens for the cyclohexadienyl-arene Fe(I) derivatives with respect to the isoelectronic cyclopentadienyl analogues.

2.4. DFT calculations

DFT calculations now add a powerful tool to molecular redox investigations in being able to calculate the structures of difficult-to-characterize products and intermediates [21]. Reduction and oxidation of the cyclopentadienyl complex **3**$^+$ leads to elongation of both Fe···ring distances. In the case of reduction, the Fe···Cp distance increases (for 0.121 Å) in greater extent than Fe···C_6H_6 (for 0.033 Å). In contrast, oxidation results in stronger elongation of Fe···C_6H_6 (for 0.136 Å) than of Fe···Cp (for 0.049 Å). Redox changes practically do not affect the coplanarity of the rings in **3**$^+$. However, considerable folding of both rings upon reduction (Cp 7.0, C_6H_6 6.2°) and of the benzene ring upon oxidation (6.9°) is worth mentioning. Similar geometry changes were also predicted for the related cyclohexadienyl and pentamethylcyclopentadienyl cations **1**$^+$ and **4**$^+$. The cyclohexadienyl ligand in the former is strongly twisted upon reduction and becomes less folded upon oxidation (the folding angle is 44.1 for monocation **1**$^+$ and 26.5° for dication **1**$^{2+}$).

The different elongation of the metal-ring distances in **3**$^+$ upon reduction and oxidation can be explained on the basis of MO analysis. Indeed, SOMO of the reduced species $[CpFe(C_6H_6)]^0$ (**3**) is more antibonding for the interaction of iron with Cp than with benzene, Fig. 8. The SOMO of the oxidized species $[CpFe(C_6H_6)]^{2+}$ (**3**$^{2+}$), which has mainly d_{z2} character, is essentially nonbonding and cannot be responsible for geometry changes.

The explanation comes from the significant change of δ-type orbitals having main contribution from d_{xz} and $d_{x^2-y^2}$ metal orbitals. As shown in Fig. 9a, in monocation **3**$^+$ such orbitals (HOMO−1, HOMO−2) are responsible for strong M → C_6H_6 back donation. On the contrary, in dication **3**$^{2+}$ the respective orbitals (HOMO, HOMO−3) are essentially nonbonding in accordance with the increase of metal oxidation state, explaining strong loosening of the Fe–C_6H_6 bond.

In addition, inclusion of solvation effects into energy calculations makes possible the evaluation of redox potentials, which has already found wide application for inorganic and organic compounds. However, only a few examples of such calculations for organometallic compounds are described in the literature [22]. Table 3 compares the experimental and the calculated formal electrode potentials for the complexes studied together with those of a few ferrocene derivatives. Independently from the solvation model (PCM or COSMO), computation satisfactory predicts the redox potentials for reversible processes (the maximum deviation from experimental values is 0.25 V). In contrast, the calculated potentials for irreversible processes are strongly different from the experimental ones, also in view of the non thermodynamic meaning of such experimental values [17].

2.5. Mössbauer effect study

^{57}Fe Mössbauer effect spectra (MES) were acquired at various temperatures in transmission geometry. Except as noted below, all spectra consisted of well resolved doublets, and the line widths (fwhm) were generally in the area of 0.232 ± 0.007 mm s^{-1}. The hyperfine parameters at 90 K [isomer shift IS(90) and quadrupole splitting, QS(90)] are summarized in Table 4, together with derived quantities as will be noted. A typical spectrum in zero field is shown in the upper trace of Fig. 10.

(a) Compound ***1****PF*$_6$: The IS is very similar to that of the parent ferrocene, but the QS has only about one half the value usually observed in ferrocenoid complexes. The temperature dependence of the IS shows some curvature at low temperatures but the data (9 data points) in the interval 174 < *T* < 280 K are well fitted by a linear regression as noted in Table 3. From this temperature dependence the calculated value for the effective vibrating mass (M_{eff}) [23] is 87 ± 3 daltons in reasonable agreement with previously reported values [24]. Similarly, the temperature dependence of the ln area under the resonance curve, $-\mathrm{d}\ln A/\mathrm{d}T$, in the high temperature limit is well fitted by a linear regression. From the two temperature dependencies the Mössbauer lattice temperature, Θ_M [2423] is found to be 89 ± 3 K. The area ratio, $R = A(+)/A(-)$, where $A(+)$ and $A(-)$ are the areas at more positive and more negative velocities

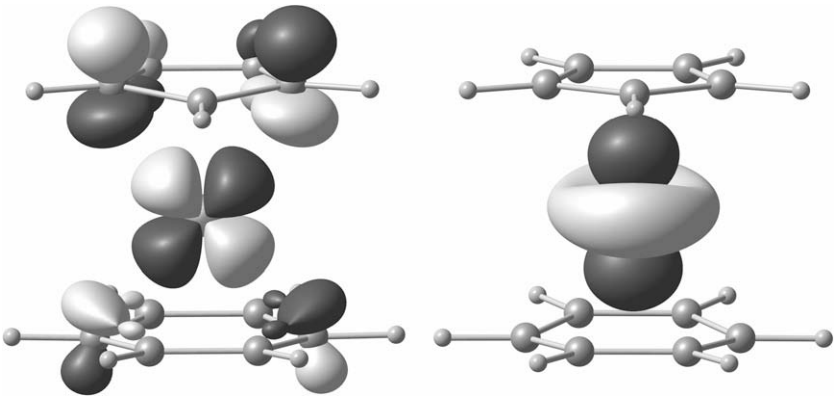

Fig. 8. SOMOs of $[CpFe(C_6H_6)]^0$ (**3**) (left) and $[CpFe(C_6H_6)]^{2+}$ (**3**$^{2+}$) (right).

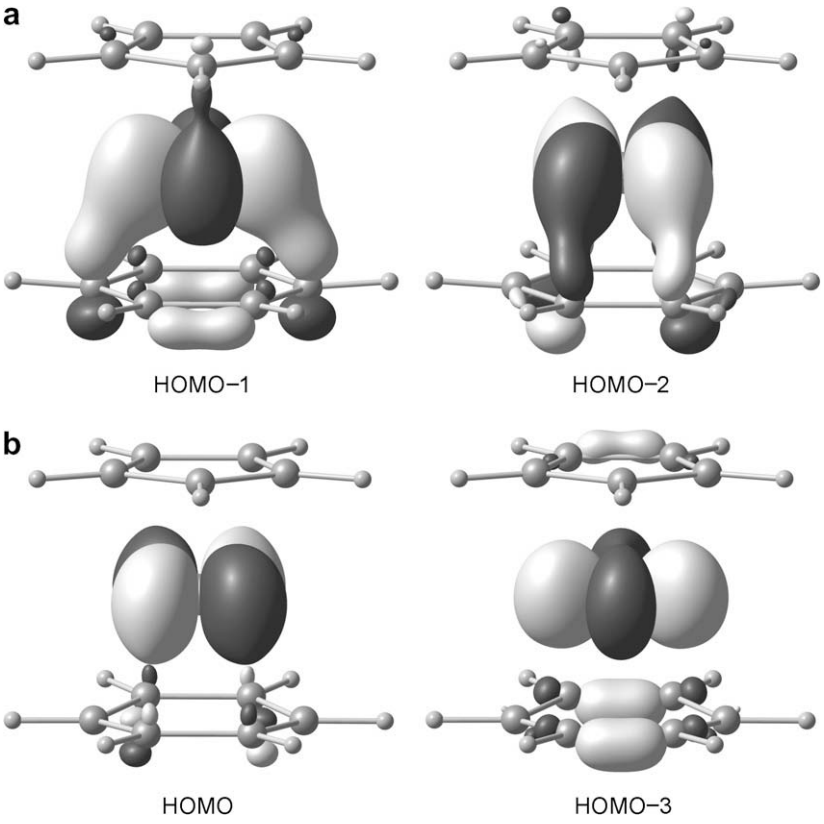

Fig. 9. δ-Type orbitals of: (a) monocation $\mathbf{3}^{+}$; (b) dication $[CpFe(C_6H_6)]^{2+}$ ($\mathbf{3}^{2+}$).

than the spectrum centroid, respectively, is temperature independent up to about 180 K and then evidences vibrational anisotropy as noted earlier [25]. This observation is consistent with the fact that the temperature dependence of the QS parameter undergoes a significant change at ~180 K, as is also true of $-\mathrm{d}\ln A/\mathrm{d}T$. All of these data suggest a structural discontinuity at about this temperature, but the exact nature of this discontinuity, which may be related to the onset of ring rotation in the solid, is not clear from the presently available results.

(b) Compound ***2b****PF*$_6$: The ME spectrum of this compound shows the presence of a small impurity with an IS(90) of ~0.31 mm s^{-1}, but the presence of this has been corrected for in the subsequent data analysis. Replacement of the C_6H_6 ring system in **1**PF_6 by three Bu^{t}NC ligands causes the IS(90) to decrease by ~0.35 mm s^{-1} commensurate with an increase in the s-electron density at the nucleus, while the QS(90) value has changed by only about 5%. The temperature dependence of the ln$A$ shows some curvature, but the low temperature ($87 < T < 172$ K) data are well fitted by a linear regression with a slope of $-(8.18 \pm 0.16) \times 10^{-3}$ K^{-1} and a correlation coefficient of 0.998 for 5 data points. This slope permits the calculation [26] of the mean-square-amplitude-of-vibration parameter $\mathbf{F}$ ($= k^2\langle x^2_{ave}\rangle$) of 0.818 ± 0.016 at 100 K which compares

Table 3
Experimental and calculated formal electrode potentials (V, vs. SCE) for the present iron complexes and a few classical ferrocene compounds (optimized at Priroda6/PBE/L$_1$) in CH_2Cl_2 solution

Compound	Transition	$E°$ (experimental)	$E°$ (calculated)	
			COSMO [a]	PCM
$[CpFe(\eta\text{-}C_6H_6)]^+$ ($\mathbf{3}^+$)	+/0	−1.44	−1.49	−1.55[b], −1.62[c], −1.69[d]
	+/2+	–	+3.05	+2.53[b], +2.45[c], +2.49[d]
$[Cp^*Fe(\eta\text{-}C_6H_6)]^+$ ($\mathbf{4}^+$)	+/0	−1.73	−1.86	−1.88[b], −1.98[d]
	+/2+	+1.70[e]	+2.59	+2.16[b], +2.45[c], +2.18[d]
$[(\eta^5\text{-}C_6H_7)Fe(\eta\text{-}C_6H_6)]^+$ ($\mathbf{1}^+$)	+/0	−1.35	−1.20	−1.33[b], −1.44[c], −1.43[d]
	+/2+	+1.35[e]	+2.33	+1.78[b], +1.72[c], +1.74[d]
$[(\eta^5\text{-}C_6H_7)Fe(^t\mathrm{BuNC})_3]^+$ ($\mathbf{2b}^+$)	+/0	–	−1.84	−1.81[b], −1.82[d]
	+/2+	+1.07[e]	+2.01	+1.68[b], +1.62[d]
$[(\eta^5\text{-}C_6H_7)Fe\{P(OMe)_3\}_3]^+$ ($\mathbf{2c}^+$)	+/0	–	−1.56	−1.38[b], −1.41[c]
	+/2+	+1.04[e]	+1.67	+1.71[b], +1.65[c]
$FeCp_2$	0/+	+0.39	+0.59	+0.39[b], +0.32[c], +0.38[d]
$FeCpCp^*_2$	0/+	+0.04[f]	+0.22	+0.09[b], +0.06[c], +0.12[d]
$FeCp^*_2$	0/+	−0.23[f]	−0.13	−0.20[b], −0.14[d]

[a] BP86/TZ2P.
[b] BP86/6-311G(d,p) for C, H and LANL2DZ for Fe.
[c] BP86/TZVP.
[d] BP86/def2-TZVPP.
[e] Irreversible process.
[f] Ref. [48].

Table 4
Summary of Mössbauer data for the compounds discussed in the text

Compound	**3**PF_6	**4**PF_6	**1**PF_6	**2b**PF_6	**2c**PF_6	**2d**PF_6	Units
IS(90)	0.522(5)	0.510(4)	0.527(3)	0.171(3)	0.202(8)	0.225(3)	mm s^{-1}
QS(90)	1.655(5)	1.404(4)	1.353(3)	1.433(3)	1.325(8)	1.347(3)	mm s^{-1}
$-dIS/dT$	4.41(7)	Curv.	4.77(16)	Curv.	2.55(16)	2.07(2)	10^{-4} mm s^{-1} K^{-1}
$-dQS/dT$		$\sim T$ ind.			T ind.		
$-d\ln A/dT$	5.91(8)	6.45(8)	11.24(27)	12.2(3)	7.12(19)	14.4(6)	10^{-3} K^{-1}
R	0.988(11)	1.014(12)			0.995(13)		
$\mathbf{F}_{x,100}$	0.681(17)	0.770(39)		0.983(5)	0.765(8)		
$\mathbf{F}_{M,100}$	0.591(8)	0.645(8)		0.818(16)	0.712(20)	1.44(6)	

well with the $U_{i,j}$ values reported by Kudinov et al. [10] of 0.983 ± 0.005 at the same temperature. The temperature-dependent IS data show significant curvature over the whole temperature range (up to 284 K) negating the possibility of calculating Θ_M and M_{eff} for this compound.

*(c) Compound **2c**PF_6*: The ME spectra of this compound are free of any impurity contributions and the IS and ln A temperature dependencies are well fitted by linear regressions with correlation coefficients of 0.99 for 17 data points. As in the case of **2b**PF_6, replacement of the C_6H_6 ring in **1**PF_6 by the $(MeO)_3P$ ligands causes a major reduction in IS(90) but only a small reduction in QS. The hyperfine parameters and derived quantities are included in Table 3. The calculated M_{eff} value is 163 ± 9 daltons, signifying a strong covalency in the metal atom ligand interaction. The Θ_M value is 82 ± 3 K justifying the high temperature limiting assumption [23]. As was noted for **2b**PF_6, the **F** values derived from the X-ray $U_{i,j}$ data reported by Kudinov et al. [10] at 100 K and those based on the ME data are 0.765 ± 0.008 and 0.712 ± 0.020, respectively. These values are significantly smaller than the **F** values for **2b**PF_6 signifying a smaller mean-square-amplitude-of-vibration in the latter compared to the former.

*(d) Compound **2d**PF_6*: As expected the hyperfine parameters of **2d**PF_6 are very similar to those of **2c**PF_6, including the relatively small value of QS(90). The IS shows an unusual break from a low temperature slope to a high temperature slope at ~200 K, but this is not reflected in the recoil-free fraction data. It is interesting, however, to compare $-d\ln A/dT$ for **2c**PF_6 and **2d**PF_6 and this comparison is effected in Fig. 11, from which it is immediately seen that the ethyl phosphate homologue evidences a much "softer" lattice than its methyl companion. This observation is likely to be the result of the presence of low-frequency "molecular" vibrations in **2d**PF_6 superimposed on the "atomic" vibrations of the metal atom itself, since the IS parameters are nearly identical within experimental error, the difference amounting to only ~10%, whereas the slope difference is a factor of two. It has not yet been possible to examine single crystals of **2d**PF_6 by X-ray diffraction so that an independent comparison of $U_{i,j}$ values is not possible at this time. While the temperature dependence of QS is negative due to thermal expansion, as expected, the hyperfine parameters are not otherwise exceptional.

*(e) Compound **3**PF_6*: In several ways, this turns out to be the most interesting compound included in the present study. At low temperatures ($94 < T < 260$ K) the ME spectra consist, as usual, of a well resolved doublet with line widths of ~0.28 mm s^{-1}. The hyperfine parameters at 90 K are included in Table 3. The M_{eff} value evaluated from the low temperature data is 100 ± 2 daltons and Θ_M = 114 ± 2 K. The temperature dependence of **F** in the low temperature limit is well fitted by a linear regression with r = 0.99 for 8

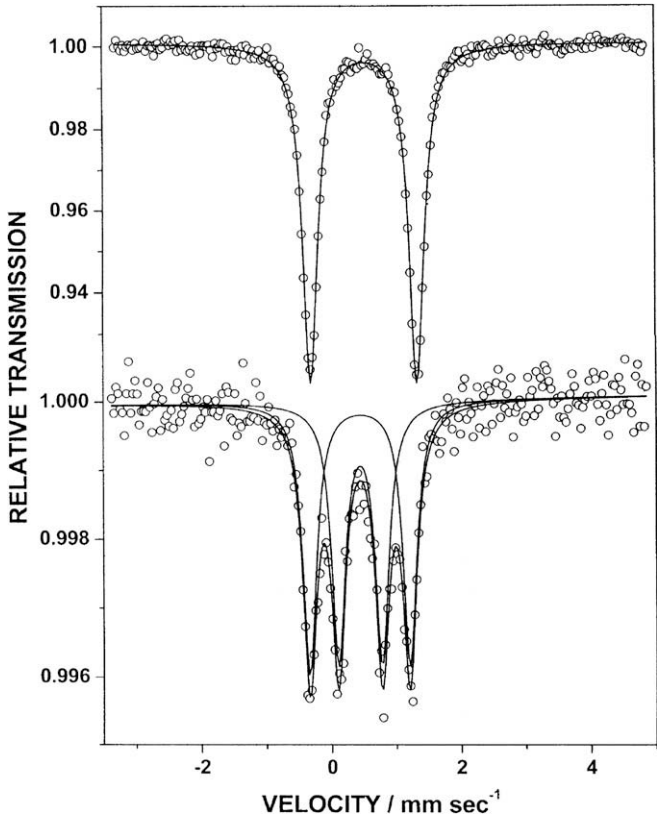

Fig. 10. ME spectra of **3**PF_6 at 109.5 K (top trace) and 310 K (bottom trace). The area ratio of the two sites in the bottom trace is 1.05:1. On further increase of temperature, this doublet of doublets collapses into a single broad resonance at $T \leqslant 315$ K, but this first order phase change is completely reversible (see text).

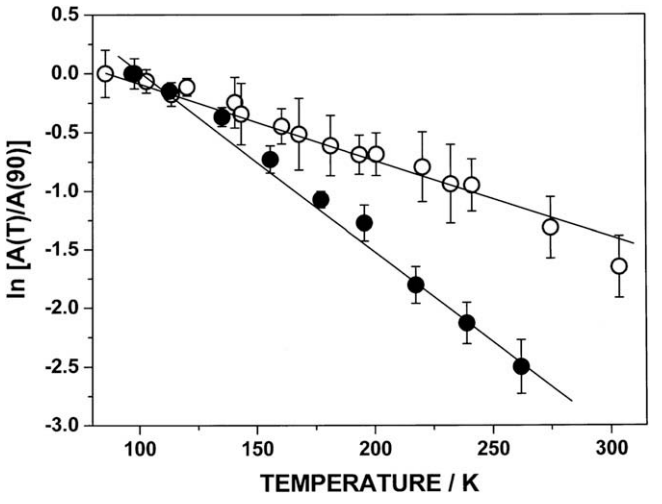

Fig. 11. Temperature dependence of the logarithm of the recoil-free fraction (normalized to the 90 K data point) for **2c**PF_6 (open data points) and **2d**PF_6 (filled data points). The larger slope of the latter data clearly indicate a "softer" lattice environment for the iron atom in **2d**PF_6 compared to **2c**PF_6.

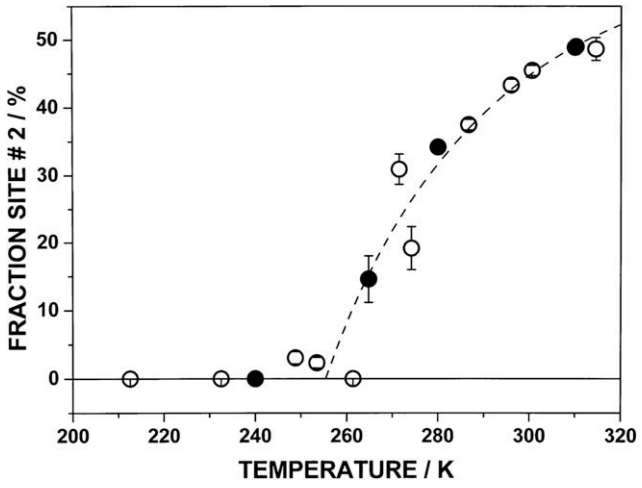

Fig. 12. Fraction of the area of the second Fe site (corresponding to the smaller QS doublet in the bottom trace of Fig. 10) of compound **3**PF_6.

data points. The value $\mathbf{f}_{M,296} = 1.75 \pm 0.02$ corresponds exactly to $\mathbf{f}_{X,296}$ evaluated from the X-ray data of Kudinov et al.

Above ~260 K, the ME data are better fitted by two doublets and the relative area under the resonance curve (corresponding to the relative population of the two sites, assuming equal recoil-free fractions) approaches 1 as $T \rightarrow 310$ K. A representative spectrum at 310 K is shown in the lower trace of Fig. 10.

This relative population is summarized graphically in Fig. 12 from which it is clear that the phase transition to a structure with two inequivalent iron sites is a second order one, in agreement with the conclusions based on the X-ray data at 296 K referred to earlier. Moreover, this second order phase transition is clearly reversible, as shown by comparison of the resonance observed on warming (open data points) and those observed on cooling from $T > 325$ K (filled data points). The hyperfine parameters at 310 K are IS(310) = 0.432 ± 0.004 and QS(310) = 1.545 ± 0.004 mm s^{-1} for the "outside" doublet, and IS(310) = 0.438 ± 0.004 and QS(310) = 0.673 ± 0.004 mm s^{-1} for the "inner" doublet reflecting the fact that the quadrupole interaction has decreased by a factor of ~2.

Below ~255 K, the ME spectra consist of a single doublet. Above this temperature, a four-line spectrum develops (see Fig. 10) and the fraction of the second Fe site approaches 50% as $T \rightarrow 315$ K. Above this latter temperature the ME spectrum consists of a broad line of about the same IS as the lower temperature data. The lower temperature transition is clearly second order. The higher temperature transition is first order and shows a small hysteresis. Clearly both phase transitions are completely reversible.

A second phase transition occurs at a temperature of ~317 K. Above this temperature, the two quadrupole doublets coalesce into a single broad line with IS(319.7) = 0.433 ± 0.011 mm s^{-1} and a line width (fwhm) of 0.325 ± 0.034 mm s^{-1}. These data, as well as the relative area under the resonance curve show unambiguously that this single line does not arise from the adventitious presence of an impurity (e.g. Fe in the windows, etc.) but indeed reflects a phase transition to a structure in which the iron atom occupies a site for which the charge distribution is nearly cubic. On warming, the two doublet nature of the ME spectrum is retained up to ~320 K. On cooling from 324 K to 315.4 K the single broad line spectrum is retained, showing the presence of a small hysteresis in the data consistent with its presumed first order character. Further cooling this sample to 310.2 K restores the four-line nature of the ME spectrum. These data suggest strongly that the second phase transition is crystallographic in origin, but the exact nature of this high symmetry form of **3**PF_6, in which the charge distribution around the Fe atom is nearly cubic, will have to be resolved by high temperature single crystal X-ray diffraction experiments.

(f) Compound ***4****PF*$_6$: The molecular composition of **4**PF_6 is identical to that of **3**PF_6 except that the Cp ring is replaced by its Cp^* homologue, and not surprisingly the hyperfine parameters at 90 K are not very different between the two compounds. Both the IS and ln*A* parameters show slight curvatures in the temperature-dependent behaviour. The low temperature data for ln A ($90 < T < 253$ K) can be well fitted to a linear regression with $r = 0.999$ for 9 data points. From this temperature dependence and the corresponding X-ray data at 100 K the two vibrational amplitude parameters are calculated to be $\mathbf{f}_{X,100} = 0.770(39)$ and $\mathbf{f}_{M,100} = 0.645(75)$. It may be conjectured that part of this difference, arises from the presence of the ring methyl groups and their steric effects with the onset of ring rotation. It is however clear from the area ratios of the two components of QS that there is little motional anisotropy in the metal atom motion parallel and perpendicular to the symmetry axis running perpendicular to the two ring ligand planes and through the metal atom.

There is, in addition, a further interesting experimental result concerning **4**PF_6 which relates to the charge state of the iron atom in this cationic complex. As has been noted copiously in the ME literature [27], one-electron oxidation of diamagnetic ferrocenoid

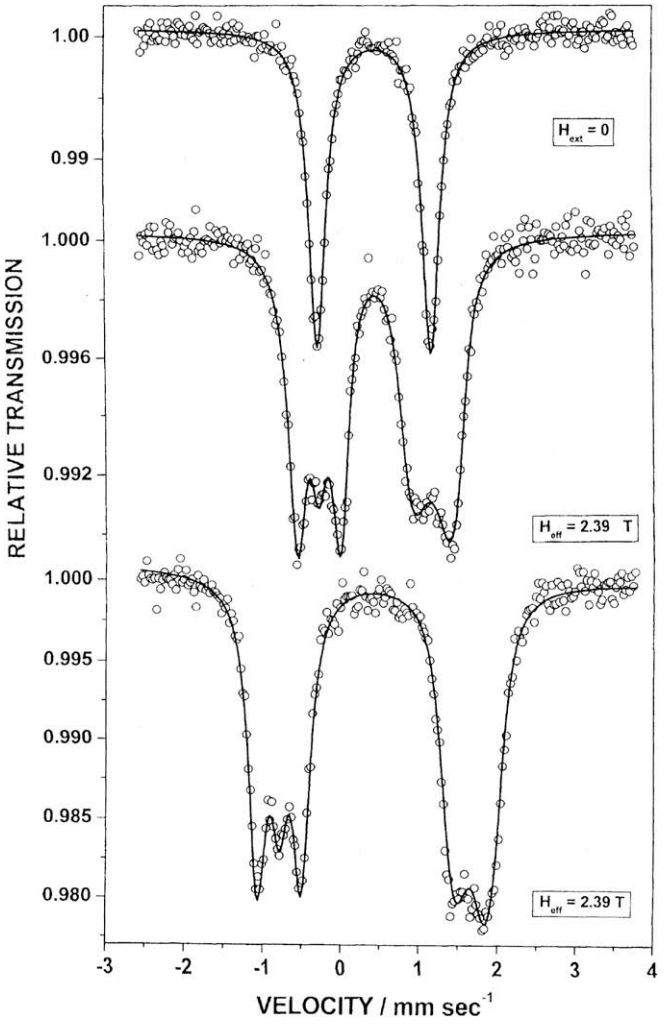

Fig. 13. Room temperature ME spectra of **4**PF_6 in the absence (top trace) and presence (middle trace) of a small magnetic field. The bottom trace is the comparison ME spectrum of ferrocene under identical conditions.

complexes leads to the almost complete collapse of the QS parameter due to the removal of an electron from the metal atom $\psi(e_{2g})$ orbital [28]. In fact the ME data showed the correctness of the molecular orbital model for ferrocene and Collins [29] concluded that in this compound QS > 0, while in the one-electron oxidation products, however, QS < 0. Following the pioneering work of Collins et al. [29] we have examined the effect of a small magnetic field on the ME spectra of both ferrocene and compound **4**PF_6 and the results are summarized graphically in Fig. 13.

The QS in ferrocene is known to be >0 and the splitting of the zero field doublet of **4**PF_6 into a lower lying triplet and higher lying doublet (middle trace) clearly shows that in this compound QS > 0 as well and that the metal atom is effectively in a diamagnetic environment.

When ME spectra of **4**PF_6 are obtained in a magnetic field [30], the normal narrow line doublet (upper trace of Fig. 13) is split into a lower energy triplet and a higher energy doublet (middle trace). From this figure it is seen that the sign of QS is positive in both ferrocene (lowest trace of Fig. 13) and **4**PF_6, and that under identical experimental conditions, the magnitude of the hyperfine field is the same in both cases. It thus follows that the electron leading to the cationic nature of the metal containing fragment in **4**PF_6 is NOT removed from one of the iron d-orbitals, and that the local environment of the metal atom is primarily diamagnetic. The reduction in QS from decamethyl ferrocene [QS(90) = 2.473(2) mm s^{-1}] to the value observed in **4**PF_6 [QS(90) = 1.404(4) mm s^{-1}] must then be ascribed to the presence of one Cp^* ring by its C_6H_6 replacement.

3. Conclusion

As happens for $[CpFe(\eta\text{-}C_6H_6)]^+$ and $[(\eta\text{-}C_4Me_4)Co(\eta\text{-}C_6H_6)]^+$, the benzene ligand in the (cyclohexadienyl)iron complex $[(\eta^5\text{-}C_6H_7)Fe(\eta\text{-}C_6H_6)]^+$ (**1**$^+$) is replaced by 2-electron donor ligands L (such as MeCN, tBuNC, $P(OMe)_3$, $P(OEt)_3$) under visible light irradiation. Therefore, **1**$^+$ can be used as a synthon of the $[(\eta^5\text{-}C_6H_7)Fe]^+$ fragment, as illustrated by the preparation of the tris(ligand) piano-stool derivatives $[(\eta^5\text{-}C_6H_7)FeL_3]$ (**2a**$^+$–**d**$^+$). Such piano-stool Fe(II) complexes undergo one-electron reduction and oxidation processes to the corresponding Fe(I) and Fe(III) species, respectively, which however are markedly less stable that the cyclopentadienyl analogues. Computation predicts quite satisfactory the redox potentials for the pertinent electron-transfer processes displaying features of complete or partial chemical reversibility.

Temperature-dependent Mössbauer effect (ME) spectroscopy has been used to elucidate the charge state and vibrational dynamics of the iron atoms in the subject compounds. In general, there is good agreement between the ME and X-ray data pertaining to the mean-square-amplitudes-of-vibration of the metal atoms. The ME data also document the presence of two phase transitions in **3**$^+$ and confirm the fact that the QS is positive in **4**$^+$. Evidence for non-isotropic metal atom motion is also presented for several of the compounds examined in this study.

4. Experimental

4.1. General

The reactions were carried out under an inert atmosphere in dry solvents. The isolation of products was conducted in air. Complexes **1**PF_6 [10], **3**PF_6 [31], and **4**PF_6 [14a] were prepared as described in the literature. ^1H and $^{31}P\{^1H\}$ NMR spectra were recorded with a Bruker Avance-400 spectrometer operating at 400.13 and 161.98 MHz, respectively. Materials and apparatus for electrochemistry have been described elsewhere [32]. Under the present experimental conditions the one-electron oxidation of ferrocene occurs at $E^{\circ\prime} = +0.39$ V.

4.2. Synthesis of tris(ligand) complex **2b**–**d**PF_6

Acetonitrile (3 ml) was added to mixture of **1**PF_6 (80 mg, 0.223 mmol) and ^{t}BuNC or $P(OR)_3$ (0.15 ml) in a Schlenk tube (d = 15 mm). The reaction mixture was irradiated for 6 h with a 400 W high-pressure mercury vapor lamp with a phosphor-coated bulb. Both the tube and the lamp were placed into a vessel of an appropriate volume covered inside with aluminium foil; cooling was accomplished with running water. The solvent was removed in vacuo and the residue was filtered in CH_2Cl_2 through a layer of Al_2O_3 (3–5 cm). Yellow solution obtained was evaporated for ca. 2 ml. Ether (ca. 10 ml) was added to precipitate a yellow solid.

2bPF_6, L = ^{t}BuNC, yield 89 mg (75%). ^1H NMR ([D_6]acetone): δ = 6.34 (m, 1H, C_6H_7), 4.90 (m, 2H, C_6H_7), 2.87 (m, 2H, C_6H_7), 2.54 (m, 1H, C_6H_7), 1.51 (m, 27H, ^{t}BuNC) ppm. Anal. Calc. for $C_{21}H_{34}F_6FeN_3P$ (529.33): C, 47.64; H, 6.47; N, 7.94. Found: C, 47.82; H, 6.47; N, 7.92%.

2cPF_6, L = $P(OMe)_3$, yield 115 mg (79%). ^1H NMR ([D_6]acetone): δ = 6.29 (m, 1H, C_6H_7), 5.01 (m, 2H, C_6H_7), 3.80 (s, 27H, Me), 2.86 (m, 2H, C_6H_7), 1.52 (m, 1H, C_6H_7) ppm. $^{31}P\{^1H\}$ NMR ([D_6]acetone): δ = 169.8 (s, 3P, $P(OMe)_3$), −144.3 (sept, 1P, PF_6) ppm. Anal. Calc. for $C_{15}H_{34}F_6FeO_9P_4$ (652.16): C, 27.63; H, 5.25. Found: C, 27.41; H, 5.27%.

2dPF_6, L = $P(OEt)_3$, yield 87 mg (50%). ^1H NMR ([D_6]acetone): δ = 6.13 (m, 1H, C_6H_7), 4.95 (m, 2H, C_6H_7), 4.19 (q, 18H, Et), 2.76 (m, 2H, C_6H_7), 1.49 (m, 1H, C_6H_7), 1.33 (t, 27H, Et) ppm. $^{31}P\{^1H\}$ NMR ([D_6]acetone): δ = 164.5 (s, 3P, $P(OEt)_3$), −144.3 (sept, 1P, PF_6) ppm. Anal. Calc. for $C_{36}H_{52}F_6FeO_9P_4$ (922.51): C, 37.03; H, 6.73. Found: C, 37.07; H, 6.73%.

4.3. X-ray crystal structure determinations

Crystals of compounds **2c**PF_6, **3**PF_6 and **4**PF_6 were grown up by slow diffusion of ether into solutions of the complexes in CH_2Cl_2. The principal crystallographic data, procedures for collecting experimental data, and characteristics of structure refinement are listed in Table 1. Single-crystal X-ray diffraction experiments were carried out with a Bruker SMART APEX2 CCD area detector, using graphite monochromated Mo Kα radiation (λ = 0.71073 Å) at 100–296 K. Absorption corrections were integrated using APEX2 software [33]. The structures were solved by direct method and refined by the full-matrix least-squares against F^2_{hkl} in isotropic approximation (for non-hydrogen atoms) in the high temperature experiment **3**PF_6 and in the anisotropic approximation for other structures. Cp and C_6H_6 molecules in the structure of **3**PF_6 were refined as rigid groups. All hydrogen atoms in structures were placed in geometrically calculated positions and included in the final refinement using the "riding" model with the $U_{iso}(H)$ parameters equal to 1.2 $U_{eq}(C_i)$ or 1.5 $U_{eq}(C_{ii})$, where $U(C_i)$ and $U(C_{ii})$ are, respectively, the equivalent thermal parameters of the methyne or methylene and methyl carbon atoms to which corresponding H atoms are bonded. All calculations were performed on an IBM PC/AT using the SHELXTL PLUS 5 software [34].

4.4. Mössbauer effect spectroscopy

The air-stable powdered samples were transferred to plastic sample holders and examined in transmission geometry as described previously [25,35]. Spectrometer calibration was effected with an absorber of α-Fe at room temperature, and all isomer shifts are referred to the centroid of such calibration spectra. The "in-field" magnetic measurements were carried out at room tempera-

ture as previously described [30], and the data were evaluated using the program detailed earlier.

4.5. Computational details

Geometry optimizations were performed without constraints using PBE exchange-correlation functional [36], the scalar-relativistic Hamiltonian [37], atomic basis sets of generally-contracted GAUSSIAN functions [38], and a density-fitting technique [39] as implemented in a recent version of Priroda code [40]. The all-electron double-ζ basis set L1 augmented by one polarization function [37,41] was used. The optimized geometries of cations $\mathbf{3}^{+}$, $\mathbf{4}^{+}$, and $\mathbf{2c}^{+}$ are in a good correlation with X-ray experimental data, confirming reliability of the results.

The redox potentials relative to SCE (E°_{redox}) were calculated using $E^{\circ}_{redox} = [-(E_{red} - E_{ox}) - 4.68]/n$, where E_{red} and E_{ox} are energies (in eV) of the reduced and oxidized species including solvation and n is the number of electrons (equal to 1 in our case). The value 4.68 corresponds to the absolute potential of the reference electrode (SCE) [42]. The solvent (CH_2Cl_2) effects were included using either the polarizable continuum model (PCM) [43] or the conductor like screening model (COSMO) [44]. The PCM and COSMO calculations were performed by GAUSSIAN 03 [45] and ADF 2006.01 [46] programs, respectively. The default settings were employed in both cases. The CHEMCRAFT program [47] was used for molecular modeling and visualization.

Supplementary material

CCDC 692767, 692769, 692768 and 692770 contain the supplementary crystallographic data for **2c**PF_6, **3**PF_6, **3**PF_6 and **4**PF_6. These data can be obtained free of charge from The Cambridge Crystallographic Data Centre via www.ccdc.cam.ac.uk/data_request/cif.

Acknowledgements

Financial support from the Division of General Chemistry and Material Sciences of RAS and the University of Siena (PAR 2005) is gratefully acknowledged. The authors are indebted to Dr. S. Cohen of the Hebrew University for helpful discussions concerning the X-ray data. A.V.V. thanks the President of the Russian Federation for the Grant (Project MK-966.2008.3).

References

[1] T.P. Gill, K.R. Mann, Inorg. Chem. 19 (1980) 3007.
[2] J.R. Aranzaes, D. Astruc, Inorg. Chim. Acta 361 (2008) 1.
[3] M.V. Butovskii, U. Englert, A.A. Fil'chikov, G.E. Herberich, U. Koelle, A.R. Kudinov, Eur. J. Inorg. Chem. (2002) 2656.
[4] A.R. Kudinov, E.V. Mutseneck, D.A. Loginov, Coord. Chem. Rev. 248 (2004) 571.
[5] A.R. Kudinov, M.I. Rybinskaya, Yu.T. Struchkov, A.I. Yanovskii, P.V. Petrovskii, J. Organomet. Chem. 336 (1987) 187.
[6] A.R. Kudinov, D.V. Muratov, M.I. Rybinskaya, P.V. Petrovskii, A.V. Mironov, T.V. Timofeeva, Yu.L. Slovokhotov, Yu.T. Struchkov, J. Organomet. Chem. 414 (1991) 97.
[7] E.V. Mutseneck, D.A. Loginov, D.S. Perekalin, Z.A. Starikova, D.G. Golovanov, P.V. Petrovskii, P. Zanello, M. Corsini, F. Laschi, A.R. Kudinov, Organometallics 23 (2004) 5944.
[8] E.V. Mutseneck, D.S. Perekalin, J. Holub, Z.A. Starikova, P.V. Petrovskii, P. Zanello, M. Corsini, B. Stibr, A.R. Kudinov, Organometallics 25 (2006) 2419.
[9] A.R. Kudinov, D.A. Loginov, P.V. Petrovskii, Izv. Akad. Nauk Ser. Khim. (2007) 1864 [Russ. Chem. Bull. 56 (2007) 1930 (Engl. Transl.)].
[10] Preliminary account of this work: D.A. Loginov, M.M. Vinogradov, Z.A. Starikova, P.V. Petrovskii, A.R. Kudinov, Izv. Akad. Nauk Ser. Khim. (2007) 2088 [Russ. Chem. Bull. 56 (2007) 2162 (Engl. Transl.)].
[11] T.P. Gill, K.R. Mann, Inorg. Chem. 22 (1983) 1986.
[12] B. Klingert, G. Rihs, Organometallics 9 (1990) 1135.
[13] C.-L. Yang, Sh.-G. Ma, J.-G. Qin, D.-Y. Liu, B.-Sh. Luo, Chem. J. Chin. Univ. 19 (1998) 61 (Chinese Edition).
[14] (a) J.-R. Hamon, D. Astruc, P. Michaud, J. Am. Chem. Soc. 103 (1981) 758;
(b) D. Astruc, Tetrahedron 39 (1983) 4027;
(c) A. Darchen, J. Organomet. Chem. 302 (1986) 389;
(d) M. Lacoste, D. Astruc, J. Chem. Soc., Chem. Commun. (1987) 667;
(e) D. Astruc, Chem. Rev. 88 (1988) 1189;
(f) M. Lacoste, H. Rabaa, D. Astruc, A. Le Beuze, J.-Y. Saillard, G. Précigoux, C. Courseille, N. Ardoin, W. Bowyer, Organometallics 8 (1989) 2233;
(g) Z.J. Karpinski, J.K. Kochi, J. Organomet. Chem. 437 (1992) 211;
(h) D. Astruc, J. Organomet. Chem. 689 (2004) 4332.
[15] (a) P.M. Treichel, D.A. Komar, J. Organomet. Chem. 206 (1981) 77;
(b) J. Ruiz, M. Lacoste, D. Astruc, J. Am. Chem. Soc. 112 (1990) 5471;
(c) C. Roger, P. Hamon, L. Toupet, H. Rabaâ, J.-Y. Saillard, J.-R. Hamon, C. Lapinte, Organometallics 10 (1991) 1045.
[16] N. El Murr, J. Chem. Soc., Chem. Commun. (1981) 251.
[17] P. Zanello, Inorganic Electrochemistry. Theory, Practice and Application, RS.C, United Kingdom, 2003.
[18] J.L. Atwood, S.D. Christie, M.D. Clerk, D.A. Osmond, K. Craig Sturge, M.J. Zaworotko, Organometallics 11 (1992) 337.
[19] R.E. Lehman, J.K. Kochi, J. Am. Chem. Soc. 113 (1991) 501.
[20] K. Michkova, A. Schneider, H. Gerhard, N. Popovska, I. Jipa, M. Hofmann, U. Zenneck, Appl. Catal. A: Gen. 315 (2006) 83.
[21] W.E. Geiger, Organometallics 26 (2007) 5738.
[22] (a) M.-H. Baik, R.A. Friesner, J. Phys. Chem. A 106 (2002) 7407;
(b) M. Cossi, M.F. Iozzi, A.G. Marrani, T. Lavecchia, P. Galloni, R. Zanoni, F. Decker, J. Phys. Chem. B 110 (2006) 22961;
(c) A. Nafady, P.J. Costa, M.J. Calhorda, W.E. Geiger, J. Am. Chem. Soc. 128 (2006) 16587;
(d) D. Chong, D.R. Laws, A. Nafady, P.J. Costa, A.L. Rheingold, M.J. Calhorda, W.E. Geiger, J. Am. Chem. Soc. 130 (2008) 2692.
[23] R.H. Herber, in: R.H. Herber (Ed.), Chemical Mössbauer Spectroscopy, Plenum Press, New York, 1984, pp. 200–216.
[24] R.H. Herber, I. Nowik, V. Kahlenberg, H. Kopacka, H. Schottenberger, Eur. J. Inorg. Chem. (2006) 3255.
[25] (a) R.H. Herber, I. Nowik, Solid State Sci. 4 (2002) 691;
(b) R.H. Herber, I. Nowik, M. Rosenblum, Organometallics 21 (2002) 846;
(c) R.H. Herber, I. Nowik, M. Iyoda, J. Organomet. Chem. 658 (2002) 210;
(d) I. Nowik, R.H. Herber, J. Phys. Chem. Solids 64 (2003) 313.
[26] R.H. Herber, I. Nowik, J.O. Grosland, R.G. Hadt, V.N. Nemykin, J. Organomet. Chem. 693 (2008) 1850.
[27] H. Schottenberger, K. Wurst, U.J. Griesser, R.K.R. Jetti, G. Laus, R.H. Herber, I. Nowik, J. Am. Chem. Soc. 127 (2005) 6795. and references therein.
[28] N.N. Greenwood, T.C. Gibb, Mössbauer Spectroscopy, Chapman Hall Ltd., London, 1971.
[29] (a) R.L. Collins, J. Chem. Phys. 42 (1965) 1072;
(b) R.L. Collins, J.C. Travis, in: I.J. Gruverman (Ed.), Mössbauer Effect Methodology, 3, Plenum Press, New York, 1967, p. 123. and references therein.
[30] I. Nowik, R.H. Herber, Eur. J. Inorg. Chem. (2006) 5069.
[31] A.N. Nesmeyanov, N.A. Vol'kenau, I.N. Bolesova, L.S. Polkovnikova, Koord. Khim. 1 (1975) 1252 [Sov. J. Coord. Chem. 1 (1975) (Engl. Transl.)].
[32] D.A. Loginov, M.M. Vinogradov, Z.A. Starikova, E.A. Petrovskaya, P. Zanello, F. Laschi, F. Rossi, A. Cinquantini, A.R. Kudinov, J. Organomet. Chem. 692 (2007) 5777.
[33] APEX2 Software Package, Bruker AXS Inc., 5465, East Cheryl Parkway, Madison, Wisconsin, USA, 2005.
[34] SHELXTL v. 5.10, Structure Determination Software Suite, Bruker AXS, Madison, Wisconsin, USA, 1998.
[35] (a) I. Nowik, R.H. Herber, Inorg. Chim. Acta 310 (2000) 191;
(b) G. Laus, H. Schottenberger, K. Wurst, R.H. Herber, V. Griesser, J. Phys. Chem. B 108 (2004) 5082.
[36] J.P. Perdew, K. Burke, M. Ernzerhof, Phys. Rev. Lett. 77 (1996) 3865.
[37] K.G. Dyall, J. Chem. Phys. 100 (1994) 2118.
[38] D.N. Laikov, Chem. Phys. Lett. 416 (2005) 116.
[39] D.N. Laikov, Chem. Phys. Lett. 281 (1997) 151.
[40] D.N. Laikov, Yu.A. Ustynyuk, Izv. Akad. Nauk Ser. Khim. (2005) 804 [Russ. Chem. Bull. 54 (2005) 820 (Engl. Transl.)].
[41] E.Ya. Misochko, A.V. Akimov, V.A. Belov, D.A. Tyurin, D.N. Laikov, J. Chem. Phys. 127 (2007) 084301.
[42] S. Trasatti, Pure Appl. Chem. 58 (1986) 955.
[43] S. Miertš, E. Scrocco, J. Tomasi, Chem. Phys. 55 (1981) 117.
[44] A. Klamt, G. Schüürmann, J. Chem. Soc., Perkin Trans. 2 (1993) 799.
[45] M.J. Frisch, G.W. Trucks, H.B. Schlegel, G.E. Scuseria, M.A. Robb, J.R. Cheeseman, J.A. Montgomery Jr., T. Vreven, K.N. Kudin, J.C. Burant, J.M. Millam, S.S. Iyengar, J. Tomasi, V. Barone, B. Mennucci, M. Cossi, G. Scalmani, N. Rega, G.A. Petersson, H. Nakatsuji, M. Hada, M. Ehara, K. Toyota, R. Fukuda, J. Hasegawa, M. Ishida, T. Nakajima, Y. Honda, O. Kitao, H. Nakai, M. Klene, X. Li, J.E. Knox, H.P. Hratchian, J.B. Cross, C. Adamo, J. Jaramillo, R. Gomperts, R.E. Stratmann, O. Yazyev, A.J. Austin, R. Cammi, C. Pomelli, J.W. Ochterski, P.Y. Ayala, K. Morokuma, G.A. Voth, P. Salvador, J.J. Dannenberg, V.G. Zakrzewski, S. Dapprich, A.D. Daniels, M.C. Strain, O. Farkas, D.K. Malick, A.D. Rabuck, K. Raghavachari, J.B. Foresman, J.V. Ortiz, Q. Cui, A.G. Baboul, S. Clifford, J. Cioslowski, B.B. Stefanov, G. Liu, A. Liashenko, P. Piskorz, I. Komaromi, R.L. Martin, D.J. Fox, T. Keith, M.A. Al-Laham, C.Y. Peng, A. Nanayakkara, M. Challacombe, P.M.W. Gill, B. Johnson, W. Chen, M.W. Wong, C. Gonzalez, J.A. Pople, GAUSSIAN 03, Revision B.03, GAUSSIAN, Inc., Pittsburgh PA, 2003.
[46] F.M. Bickelhaupt, E.J. Baerends, Rev. Comput. Chem. 15 (2000) 1.
[47] G.A. Zhurko, ChemCraft 1.5, <http://www.chemcraftprog.com>, 2007.
[48] P.G. Gassman, D.W. Macomber, J.W. Hershberger, Organometallics 2 (1983) 1470.